# Diagnostics and Testing to Assess the Behavior of Organic Materials at High Heat Flux

SAND2016-10464C

ALEXANDER L. BROWN[1], RYAN R. ANDERSON[2], ANTHONY TANBAKUCHI[3], DESHAWN COOMBS[1]
Fire Science and Technology Department[1]
Concentrating Solar Technologies Department[2]
Measurement Science and Engineering Department[3]
Sandia National Laboratories
PO Box 5800, MS 1135[1]
Albuquerque, NM 87185-1135

**ABSTRACT**

Pyrolysis of materials at high heat fluxes are less-well studied because the high heat flux regime is not as common to many practical fire applications. The fire behavior of organic materials in such an environment needs further characterization in order to construct models to predict the dynamics in this regime. The test regime is complicated because of the temperatures achieved and the speed at which materials decompose due to the flux condition. A series of tests has been performed that exposed a variety of materials to this environment. The resulting imagery from the tests provide some unique insights into the behavior of various materials at these conditions. Furthermore, experimental and processing techniques suggest analytical methods that can be employed to extract quantitative information from pyrolysis experiments.

**KEYWORDS:** *forensics, ignition, industrial fires, high heat flux fires*

## INTRODUCTION

High heat fluxes are endemic to several types of fires that are not typical of domestic scenarios, but may be readily found in industrial, military, or manufacturing applications. Such applications include thermite reactions, metal fires, nuclear detonation induced fires, laser heating, explosives, propellant fires, etc. Some of these applications have practical reasons to be studied, as they can be components of a system behavior that needs to be characterized for a particular scenario, usually involving safety. We are interested in the response of a variety of solid materials to very high heat fluxes. The responses of interest are general, including the probability of ignition, the characteristics of the product formation (including heats and rates of reactions, char, gas, and condensable products), and the state of the residual material. An end goal of this work is to develop modeling methods to predict the fire behavior of materials exposed to high heat flux scenarios. Accurate data will contribute to the ability to perform model validation, which constitutes the basis for model credibility.

Normal hydrocarbon fires typically exhibit radiative fluxes in the fire in the range of 50-200 kW/m$^2$ [1,2]. These radiative fluxes may cause organic materials to pyrolyze, converting the solid matrix to gas. Characteristic reaction times are typically reported as time to ignition or mass loss initiation which is on the order of tens of seconds for these typical fluxes [3,4]. Our application pertains to fluxes as much as two orders of magnitude higher. The resulting ignition and mass loss initiation time are not as well characterized in this regime.

Consider historical high heating rate data for some common materials. Biomass (lignocellulosic materials) reactions are reasonably characterized in this regime due to a niche interest in generating liquid transportation fuels from plant matter. It is understood that the 'fast' pyrolysis regime, which for this material constitutes heating rates greater than tens of degrees centigrade per second [5,6], preferentially yields condensable (tar) products compared to the light gas and char (solid residue) products. Some polymers have also been evaluated for fast pyrolysis [e.g. 7-9]. An abundance of recent review articles exists on pyrolysis modeling and thermal material decomposition [10-13]. However, most of these reviews are primarily focused on the lower heat flux regime.

This paper exhibits results from some tests performed for a variety of materials under high heat flux conditions. The tests described here represent some initial scoping efforts, with subsequent tests aimed at producing higher quality results for model validation. Even though the test program is not fully mature, the

quality, and significance of some of the results are thought to be unique and of scientific interest. These results are presented here to exhibit some of the distinguishing features of the flux regime, as well as provide guidance to subsequent efforts aimed at producing even higher quality data product. The methods in this paper detail a novel approach to obtain data for high heat flux ignition events.

## METHODS

We report in this paper results from four material types that were exposed to focused solar flux at the Solar Furnace facility at the National Solar Thermal Test Facility located at Sandia National Laboratories in Albuquerque, New Mexico, USA. Tests were conducted during September of 2015, at approximately standard temperature (25 C; near mid-morning), but at a low pressure characteristic of the high elevation at the laboratory (around 0.8 atm). Humidity was not recorded, but was likely quite low (25% relative humidity, characteristic of typical ambient conditions). The materials tested were:

1. White cotton fabric, 8 layers thick
2. Blue lined notebook paper, 70 pages thick
3. Pine construction lumber, 20 mm thick
4. High impact polystyrene board, 3.5 mm thick

Two tests for each sample were conducted. The materials were selected based on availability as well as on the existence of historical data for these materials. The cotton fabric and notebook paper were thought to be easily ignited based on a review of historical high radiative flux ignition data in Glasstone and Dolan [14]. Pine wood is a commonly tested material in the fire and pyrolysis community. The polystyrene board was readily available, and also was thought to represent a possible candidate material for validation testing due to the existence of reaction kinetic models in the literature [16-20]. Herein we report significant portions of the data from tests with the four materials from the above list.

### The Solar Furnace Facility

The solar furnace facility consists of a heliostat mirror that tracks the sun and directs the reflected rays to the facility. The sun rays then pass through an attenuator that consists of a set of motorized louvered panels. The rays then are reflected off a parabolic dish array of reflecting mirror elements about 7 meters in diameter to a focal point that is roughly 5 cm in diameter. A photograph of the facility is shown in Fig. 1. A schematic of the facility is shown in Fig. 2 along with a general layout of the camera positions employed during these tests. A three-axis motorized table is used to position test materials relative to the focal point and holds data acquisition instrumentation and cooling manifolds.

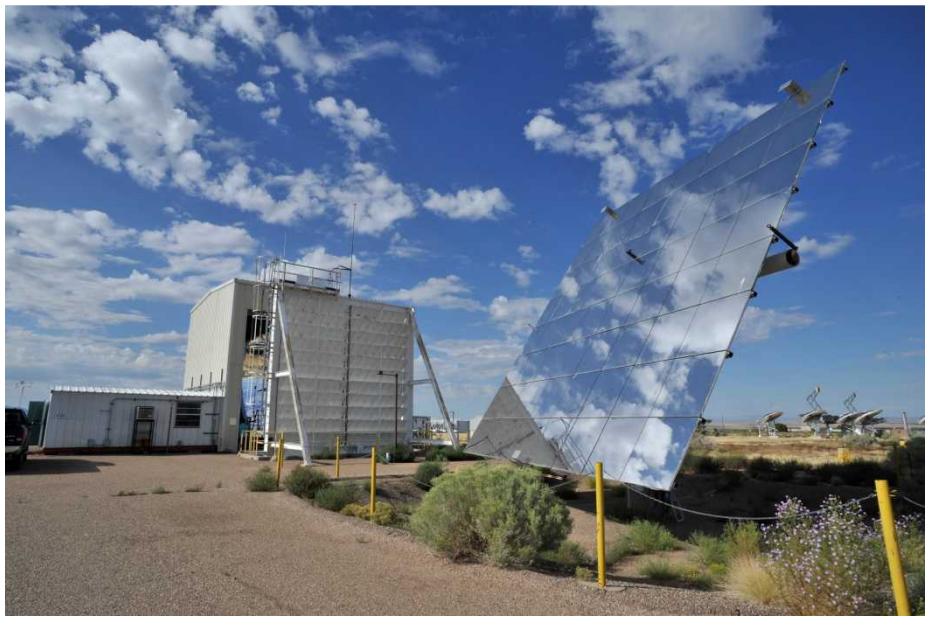

Fig. 1. A photograph of the solar furnace facility.

**Instrumentation**

Six cameras were fielded to record image frames of the decomposing materials. A general layout of the photography is found in Fig. 2. Three main types of cameras were employed. This includes:

1. FLIR SC8313 MWIR camera
2. Phantom v2511 high-speed cameras
3. Standard camcorder devices

The Phantom cameras and some of the regular cameras employed optical filters to improve the image quality during the tests. The SC8313 had a ND3 (x0.001) attenuation filter for temperatures higher than 800C. The v2511 camera that recorded results for this report had a ND1.6 (x0.025) attenuation filter. The reflected radiative flux during the tests was high, and the filters helped avoid saturated images. The high-speed and IR cameras were almost directly facing the test article faces, whereas the camcorders were positioned at oblique angles to the test article surface. All cameras were positioned at approximately the height of the target. The standard cameras had neutral density filters and were set to fast shutter speeds to prevent saturation in the product images. A pair of studio lamps were used to illuminate the target for alignment and calibration.

The flux gauge was a water-cooled circular-foil heat flux gauge with a maximum incident flux of 3,500 kW/m$^2$. It was a model TG1000 instrument from Vatell Corporation. The gauge was used to characterize the flux before and after the exposure on the test sample to provide assurance of the consistency of the flux level during the test. There was a temporal delay of about 30 seconds between the pre- and post-test flux readings, which corresponds to the time it takes to translate the table to position the flux gauge at the focal point. Were a cloud to pass in front of the sun during the test, it is expected that the pre-test and post-test flux would vary significantly over the course of the flux measurement event. The target test condition was a peak flux of 3,200 kW/m$^2$, with a constant portion of the pulse duration of approximately 2 seconds. Flux was recorded at 1 Hertz, which was not sufficiently frequent to accurately estimate a total fluence (energy per unit area). We estimate the total fluence during tests to be about 6,000-9,000 J/m$^2$. The motorized attenuators took about a second to open and close, meaning that there was an approximately linear ramp in energy of about a second before the hold at the test condition.

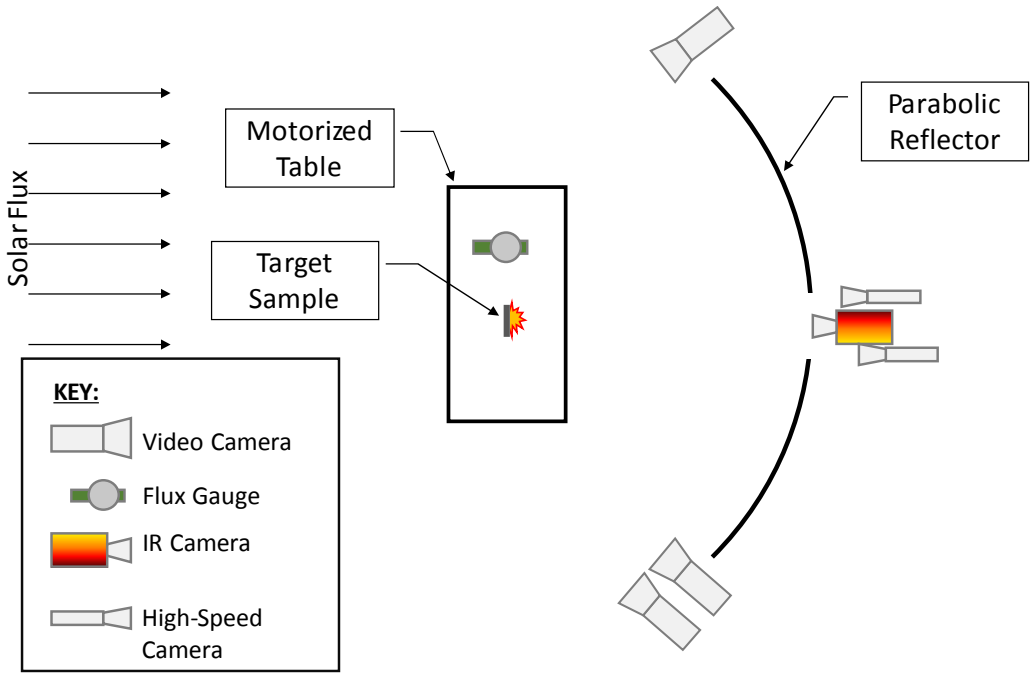


Fig. 2. A general top view lay-out of the test instrumentation.

### Image Processing

The standard video data collected comes from three cameras, two filtered cameras, to prevent saturation due to the light from the solar collector dish, and one unfiltered camera. The video data were taken at two frame rates, 30fps and 60fps. The raw video footage was taken into Adobe Premiere Pro software and a number of image sets that illustrate events of particular interest were extracted. Within Adobe Premiere the raw video footage was edited to focus on the material as the solar collector imposed heat flux. With the software, the zero time for each video was selected by finding the frame in which the first increase in the light from the opening of the solar furnace shutters can be observed on the test material. The frame immediately preceding this one was selected as the zero time. Using this as the zero time, sets of frames were pulled from each of the recorded videos that illustrate phenomena that occur during the exposure of these materials to high heat fluxes.

The second source of data for the test was the infrared camera. From the IR camera output, temperature measurements were deduced employing the hardware analytical algorithms that correlate the infrared spectral response to a corresponding object temperature.

The third source of data was the high-speed cameras. One of the cameras employed a simple ND3 filter, and yielded images based on visible emissions. These results were post-analyzed with custom motion tracking software for flow conditions. The other high-speed camera employed narrow-band IR filters. These data were not processed for this report.

## RESULTS

### Visual Images

Two softwood pine samples were tested. Results were similar, but one of the test was unique due to the grain orientation of the wood. The grains were close to parallel with the exposed surface. This resulted in images that showed the dynamic recession of the grain boundaries as the thermal flux induced a pyrolytic erosion in the material. The results of this test are shown in Fig. 3. New grains can be observed as they become visibly exposed on the surface at 1.00 seconds, 1.66 seconds, and 1.83 seconds. The grains were about 2 mm thick, so it can be inferred that the thermal flux created a crater in the wood approximately 6-8 mm deep.

The fact that the grains are visible may be unexpected if one bases their intuition on the way a wood log burns in a fire. One expects either a blackened char, a glowing red ember, or a white ash layer on the surface of burning wood. The outer rim of the flux spot exhibits char layer growth, more consistent with typical fire observations at lower flux levels. This test confirms visually the low char yield of wood at a higher heat flux condition that was described in the introduction. It also illustrates the need for experimental data in this regime where conventional lower flux derived models might not accurately predict the low char yields. Post-test, the entire surface of the exposed wood was blackened. The sample transitions back to ambient conditions through a lower flux regime that yields char. The post-test evaluation of the wood sample would have missed the low char yield that was only observable during the test. This is indicative of the value of employing imagery during these tests, and also highlights the potential for important features of high heat flux decomposition to be missed when such real-time imagery is not employed.

Although a substantial amount of wood material was pyrolyzed, the wood did not appear to ignite in any of the test video images. The pyrolysis gases appear to exhibit a sharp threshold in the image, suggesting that the test creates a gas cloud dense in pyrolysis product that is not well mixed with the surrounding air.

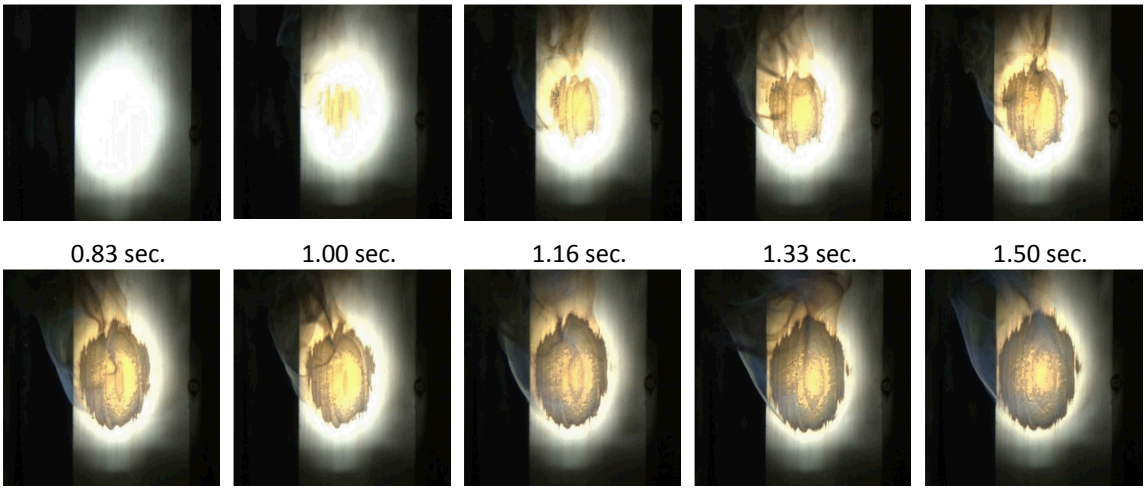

Fig. 3. Wood decomposition images at various times.

Figure 4 shows the results of the first polystyrene sample test. This material required a longer exposure to exhibit the initial off-gassing, almost ½ second longer. The pyrolysis products were largely black and opaque, with the exception of the light emissions from early in the test. The image from 1.53 seconds exhibits what was initially thought to be the start of a flaming region. The bright spot somewhat central to the black cloud was the indicator. It is a different color than the background, lending to this observation. The spot was only visible to one camera on a single frame. The second polystyrene shot was substantially different in this regard. Images from this test are found in Figure 5. The first sign of the dark pyrolysis products was about 0.15 seconds sooner, and the size of the black cloud was considerably smaller several frames after it first appeared. No evidence of the potential advent of a flame was observed. The gas cloud appears to tend towards a tear-drop shape towards the latter part of the decomposition phase for both tests. No effort was made to control the ambient wind conditions, so some of the differences between these two tests could be ascribed to variations in the ambient wind conditions. Whereas the wood grains were visible during pyrolysis for the wood test, the polystyrene appears white. This could also be suggestive of no char formation at the higher flux levels.

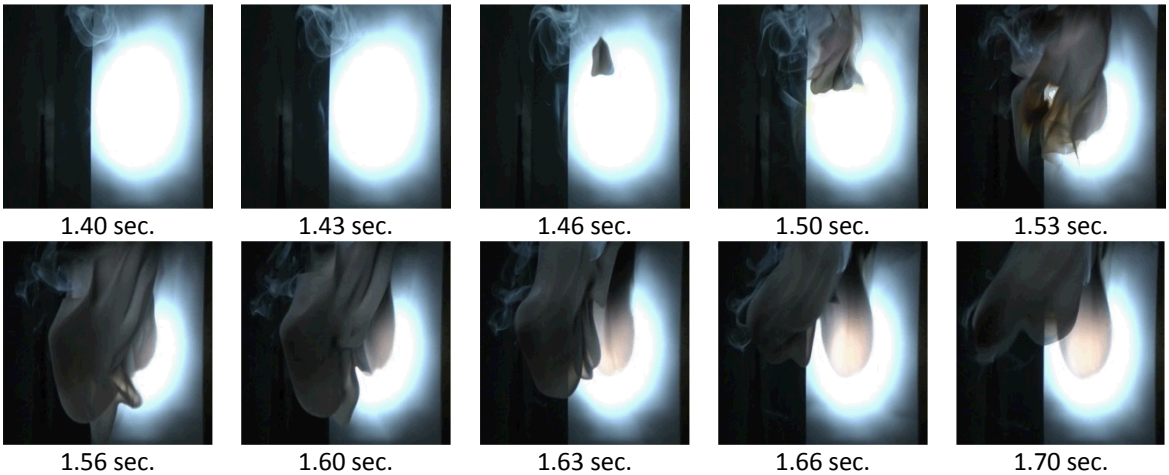

Fig. 4. Selected image frames from the first polystyrene test.

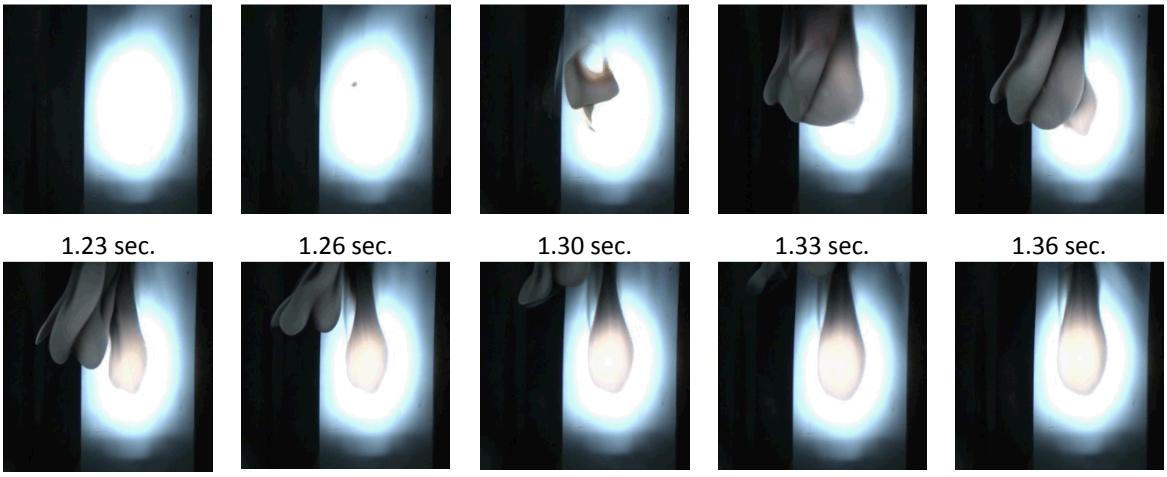


Fig. 5. Selected images frames from the second polystyrene test.

Selected frame sequences from the videos of the cotton and notebook paper tests are found in Figure 6. Both tests showed similar temporal onset of decomposition as in the wood test, about a second after exposure. Both materials were layered, and the radius of decomposition of the samples decreased with depth. Note that the paper exhibits increased charring and faster onset of charring where the ruled lines are located. The edges of the decomposition front yield some charred materials, which are ejected away from the center of the spot. The wood and polystyrene samples in contrast did not exhibit similar solid mass ejections.

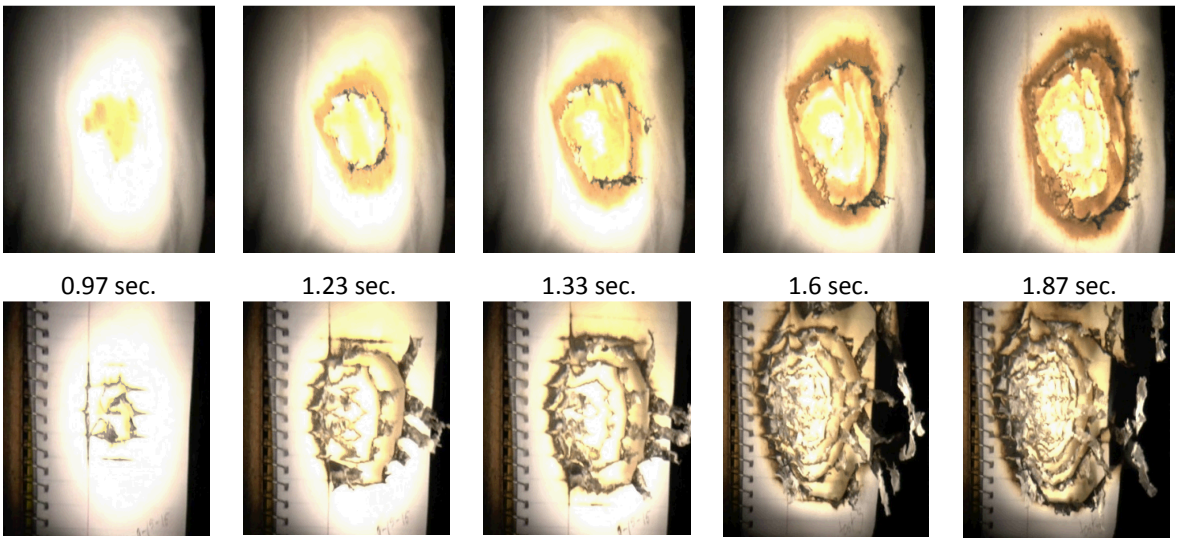


Fig.6. Cotton Fabric (top) and notebook paper (bottom) decomposition images.

**Infrared Image Analysis**

The infrared camera results were analyzed with a post-processing tool that is capable of quantifying the observed thermal behavior of the samples during exposure to the heat flux. Three tests in particular were the subject of this detailed analysis. The cameras produce a temperature from the optical signatures

collected during the test. It is normal operational procedure to calibrate the cameras to yield high accuracy temperature readings. This step was omitted from this test series, as the intent was to explore the utility of the IR imagery. This omission does not take away from the qualitative observations and methods evaluations, but should be a point of caution when interpreting the quantitative significance of the results. The potential magnitude for error is higher at lower temperatures due to the filtering and the detector requirement for a minimum number of signal counts for the interpretation of temperature. The instrument would not register temperatures below 600 K. Figure 7 shows the maximum (spatially) observed temperature of three test samples as a function of time.

A digital reticle was used to calibrate the spatial dimension for an area calculation performed on the same data, which was assessed with post-test analytical software. Figure 8 shows the area with extracted temperature greater than 1273 K (1000 ºC) for corresponding tests, as processed from the images.

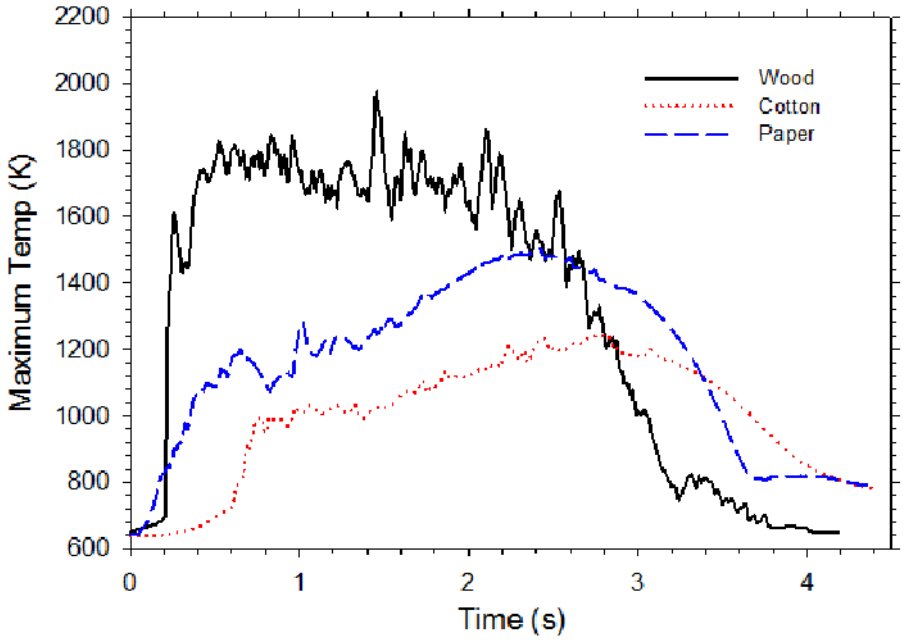


Fig. 7. Maximum temperatures from the IR video scans over time for three samples.

The temperature data illustrate how the IR camera may be used to evaluate the behavior of samples during the tests. The wood sample exhibited much higher temperatures compared to the other two samples, and the data suggest a much quicker rise in the temperature and growth of the hot area. The peak magnitude for the wood tests was surprisingly high given that the images did not indicate the presence of flaming reactions during the test. The temperature magnitudes in the range of 1600 K are consistent with flame temperatures. The cotton fabric in contrast exhibited the lowest peak temperatures and the smallest hot area. This is perhaps a function of material density. The cotton was woven and much less dense. The wood likely had a density on par with the paper, but was not a laminate material like the paper. Example IR images from two times used to produce these plots are found in Fig. 9. In all cases, the gas plume is visible above the focal spot and ascribed a temperature between that of the peak at the spot center and ambient. The semi-transparent nature of the plume of gases coming off during pyrolysis complicates the interpretation of the temperature. A calibrated temperature likely cannot be interpreted as a surface temperature due to this effect.

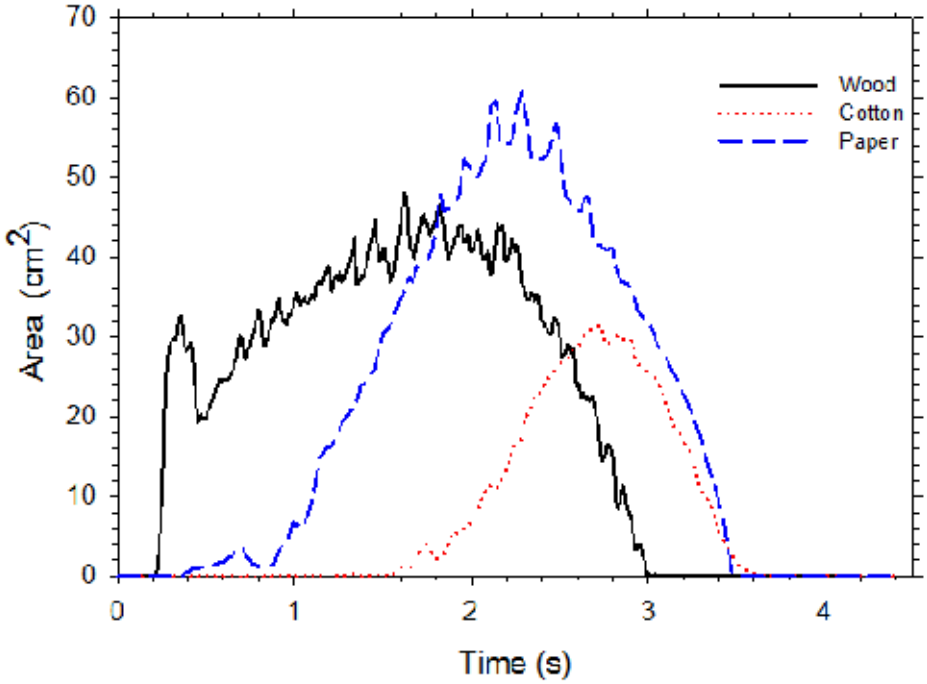


Fig. 8. Computed area with temperature greater than 1000 C versus time for three samples.

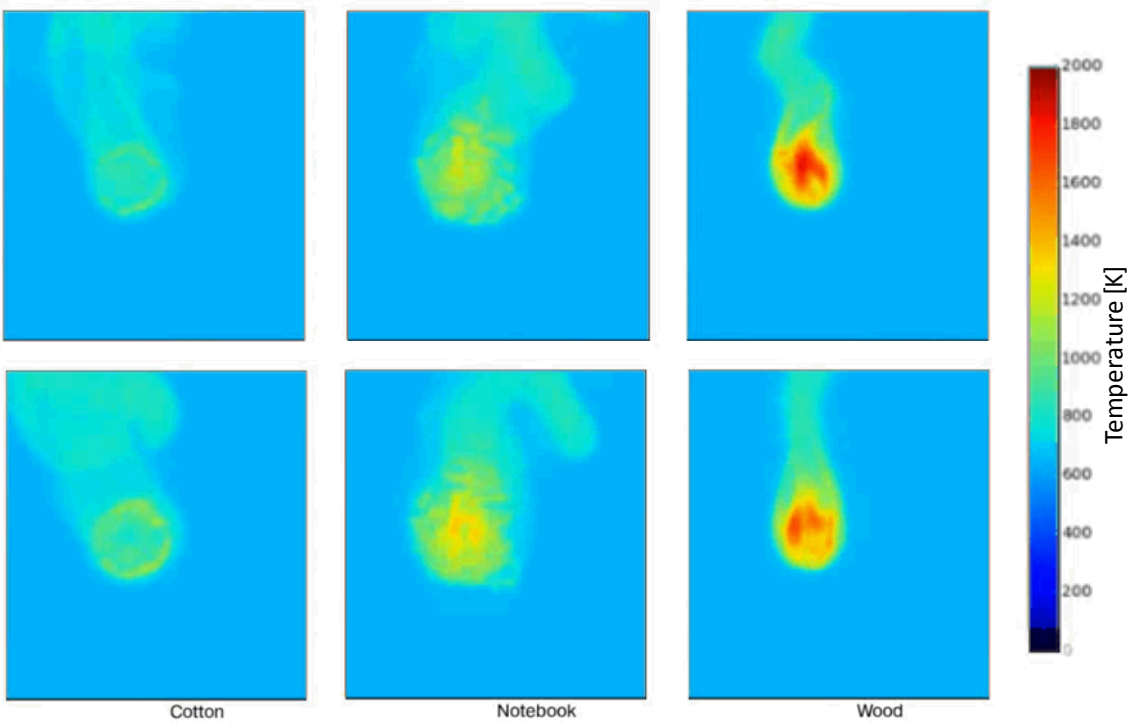


Fig. 9. IR images from the cotton, paper, and wood tests (from left to right) from early (top) and late (bottom) in the test.

**High-speed Camera Velocities**

Optical flow algorithms were used to analyze the visible high speed imagery for points that could be tracked (illustrated with purple dots in Fig. 10). By spatially calibrating the images and tracking the optical flow of the motion (shown by green vectors), a dense set of horizontal and vertical velocity data were obtained. The data can be visualized in a variety of ways. An example the corresponding instantaneous magnitudes of the velocities are shown plotted as a distribution in Fig. 11. The edges formed between consumed and unconsumed material in the layered materials made excellent points on the image for extracting velocity data. These edges are commonly detected for velocity analysis.

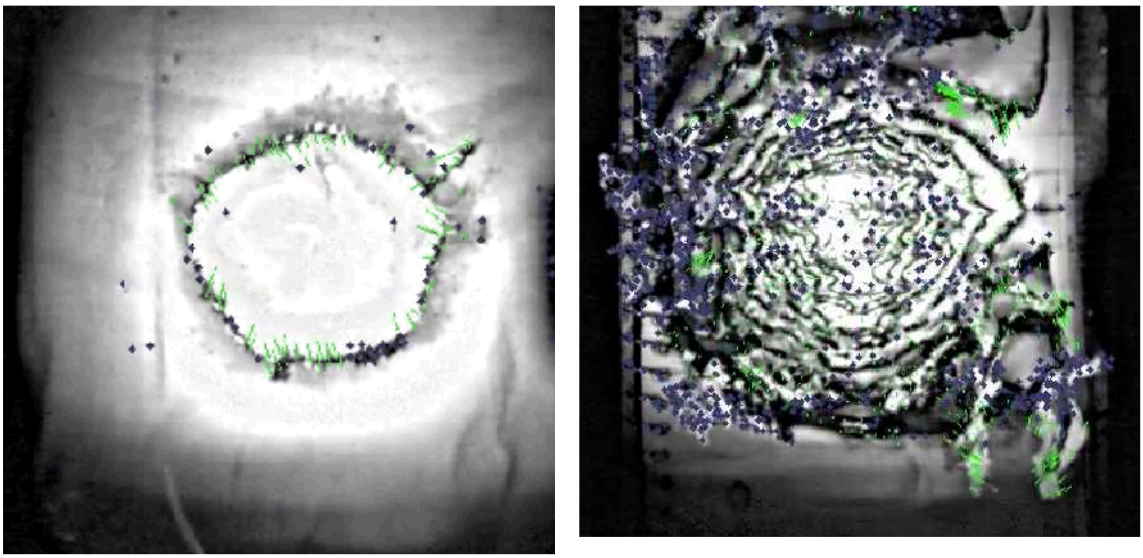

Fig. 10. Example point detection and velocity vector overlays on the cotton (left) and paper (right) images.

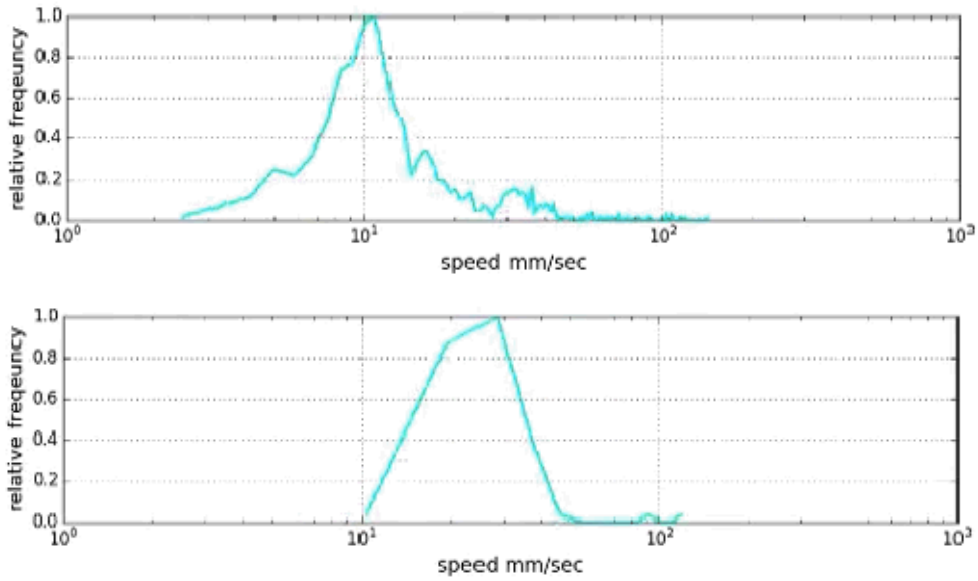


Fig. 11. Corresponding particle speed distributions for the cotton (bottom) and paper (top).

The algorithm for tracking particle speed in the tests was employed for a complete time series of results from the high speed camera images. The maximum particle speed was extracted from the same three tests analyzed in the previous section. The wood test exhibited slightly higher maximum velocities, a little over 1000 mm/sec. Figure 12 shows the maximum observed velocities over the duration of the test with the zero

time being the first detected motion. Additional calibration will be needed to coordinate these times with the times in prior figures. Because the images only deduce 2-dimensional motion, there is a potential for the maximum to be higher if the unresolved out of plane motion is significant.

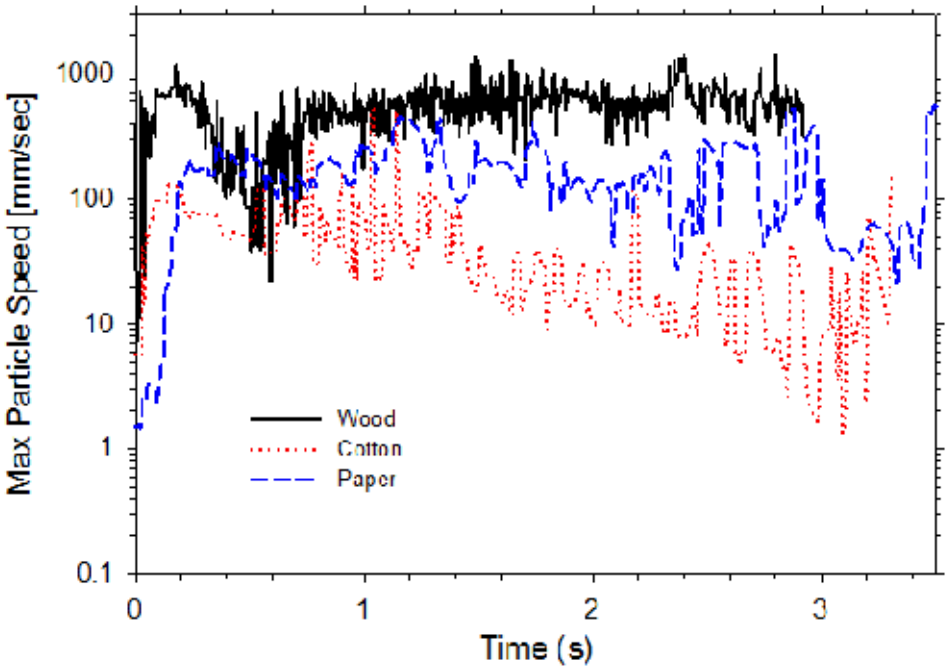


Fig. 12. Maximum particle speeds deduced from three experiments.

**DISCUSSION**

The wood decomposition video frames show the reduced char formation that occurs at higher heat fluxes. The polystyrene samples might also exhibit similar behavior, however the pyrolysis cloud was denser and obscured the surface of the sample during the test. The paper and cotton showed some signs of char formation, but like the wood this appears to be limited to peripheral edges. Some evidence of char material breaking off and flying away is evident in the videos. Details of this information is difficult to convey graphically in a written report. These tests confirm the historical observation of decreased char yields at higher heat fluxes in an air environment and help justify the need for data to better understand this phenomenology.

The char formation is thought to be an important feature relating to the fire behavior of these materials. Char formation reduces the solid mass that might otherwise vaporize and combust, but also can thermally insulate the raw material from the heat. This feature is a challenge for fire modeling efforts. Incorrectly predicting the char formation will not only affect the prediction of mass loss during a high heat flux pyrolysis event, but it also affects the potential flammability of materials that have been exposed. The visual data from these tests provide some indicators of material behavior, but suggest as well the need for increased attention to this detail in subsequent work.

The cotton, wood, and paper are cellulosic materials. This may be why they all seemed to exhibit the onset of pyrolysis at a fairly similar time relative to the initial exposure. The similarity in decomposition rate can be ascribed to both a presumed similarity in the reaction rate and the radiative absorption of the materials. The observed enhancement of the pyrolysis rate at the notebook paper lines suggests that the radiative absorption plays a role in the governing rate of decomposition. Future testing with paper should pay close attention to the radiative absorptivity, a property related to the paper color. The polystyrene sample took longer to exhibit pyrolysis products. This material was substantially different in chemical composition, as it was not cellulosic. It was also visibly white. Spectral reflectance of the polystyrene in the visible and IR

taken with a Surface Optics model 410-0038 reflectometer shows the paper has a higher reflectance in the near IR (0.6 versus 0.4), with about the same low reflectance as paper deeper in the IR (3 μm and beyond). Because of this, we infer that the delay is more likely due to differences in reaction rates of the solid matrix.

The two polystyrene tests exhibited significant variability. While the tests were conducted in a partial enclosure (a facility with an opening on one side), the air flow was subject to air fluctuations. This (turbulent effect) may have contributed to the variable plume size between the two tests. We are inclined to believe that the initiation of a flame was captured in a single frame, which exhibited a pressure expansion related to the onset of flaming. The flame was then rapidly extinguished. The differing size of the plume is one consideration leading to this inclination. A good way to explore this in the future will be to increase the number of tests in the same facility, or to find a facility with a larger exposure area. Either way, one would think that the ignition probability might go up with increased exposure area as the probability for the right conditions for sustained ignition goes up with the area exposed. Having more repeat data will also increase the likelihood of the conditions being replicated.

The paper and cotton both ignited due to the flux condition. The polystyrene may have exhibited some onset of flaming, but insufficient data exist to tell for certain. The wood did not exhibit flaming. This is consistent with historical findings for cellulosic materials from the ignition literature [5,6,8]. The video frame rate for tests like the polystyrene test should be increased in future efforts to better capture the onset of flaming. Having additional frames in the first polystyrene test would help resolve some questions regarding the material response.

Another point relating to frame rate can be made regarding the particle speed data. The maximum speed data (Fig. 12) should be helpful in designing subsequent diagnostics. The decomposition events seldom yielded velocities above 1000 mm/sec. The frequency plots shown here (Fig. 11) are representative of all the tests, and a sampling of more of these suggests more likely (peak in frequency) flow rates were 5-100 mm/sec. To our knowledge, the flow rates of gases during high heat flux decomposition have not been previously reported. These types of data should be helpful when modeling such events, as most 3D combustion models solve the Navier-Stokes equations for the local flow conditions. Validation exercises may focus on the velocity to demonstrate similarity between model predictions and experimental data. These particle speed data are also helpful for subsequent test design. Having a target flow rate means that the instrumentation settings can be optimized to sample the dynamic behavior.

The results from the IR camera were interesting, but may not be as significant to a validation effort. The expression of the image as an inferred temperature requires interpretation of the spectral response at the camera, and is not representative of precise temperatures at any one location in the test domain. The participation of the pyrolysis products and combustion products as semi-transparent media contributes to this issue. For the IR camera data to be more useful for model validation, one would need a virtual IR camera instrument model to interpret the predicted conditions in the same way the camera does from the vantage point used in these tests. The IR camera data may be more valuable if it is focused on the back side of the test object. The intervening pyrolysis products would not complicate the interpretation of the results, and the camera would be expected to give 2-dimensional thermal data.

It was noted earlier in the results section that many of the tests exhibited a pyrolysis cloud with a fairly sharp boundary in the images. We conjecture that the boundary represents a sharp transition between air and pyrolysis products. Since diffusion is a comparatively slow process, this interface can be examined in future efforts as an indicator of the location and quantity of pyrolysis product fuel. This may represent a good metric to use for validating model predictions. In follow-on efforts, we will further evaluate this by deploying cameras with different view angles to optimize the ability to extract the shape, growth rate, and position of this interface with the aim of using it to validate predictive models.

During the test series detailed in these results, a range of non-intrusive diagnostic capabilities have been exhibited. This paper has focused on the visual output from the high heat flux tests and the interpretation of the results. As a main objective of this experimental program is to develop data for model validation in the high heat flux regime, other data collection methods are being considered. Mass loss, material temperature response, and material shape will be quantified in subsequent work. Each of these are also expected to be useful target quantities to compare between models and experimental data.

## CONCLUSIONS

Video imagery and observations from a series of high heat flux pyrolysis experiments for organic materials have been presented in this paper.

- The materials exhibited minor char formation at the edges of the focal spot, but illustrate the low or total absence of char yields from organic materials at high heat flux conditions.
- The ignition of the materials was found to be consistent with historical data.
- The pyrolysis products appear to form a cloud with a sharp interface, which is a feature that can potentially be exploited for model validation.
- Analytical optical methods are introduced and employed to quantify the temperature and flow speed during the tests.
- Peak velocities were found to be around 1000 mm/sec, and most probable velocities are in the range of 5-100 mm/sec.

## ACKNOWLEDGEMENTS

The photographic set-up and operations were done with the help of Alvaro Cruz-Cabrera, Richard Simpson, Leland Sharpe, and Byron Demosthenous. Bill Kolb helped facilitate the facility work. Sarah Scott and Jeff Engerer reviewed the manuscript prior to submission. Sandia is a multiprogram laboratory operated by Sandia Corporation, a Lockheed Martin Company, for the United States Department of Energy under Contract No. DE-AC04-94AL85000.

## REFERENCES

[1] Blanchat, T., and Jernigan, D., "Fire Intensity Data for Validation of the Radiative Transfer Equation", SAND 2016-0224.

[2] Suo-Anttila, J.M. and Gritzo, L.A., "Thermal Measurements from a Series of Tests with a Large Cylindrical Calorimeter on the Leeward Edge of a JP-8 Pool Fire in Cross-Flow," Sandia report SAND 2001-1986, July 2001.

[3] Brown, J. E., Braun, E. and Twilley, W. H., "Cone Calorimeter Evaluation of the Flammability of Composite Materials," Report No. NBSIR 88-3733, National Bureau of Standards, 1988.

[4] Drysdale, D., *An Introduction to Fire Dynamics*, second edition, John Wiley and Sons, Chichester, 1999, p. 217.

[5] Milosavljevic, I. and Suuberg, E.M. (1995) "Cellulose thermal decomposition kinetics: Global mass loss kinetics," *Ind. Eng. Chem. Res.*, 34:4:1081-1091, http://dx.doi.org/10.1021/ie00043a009

[6] Graham, R.G., Bergougnou, M.A. and Overend, R.P. (1984) "Fast pyrolysis of biomass," *J. Anal. App. Pyrol.*, 6:95-135, http://dx.doi.org/10.1016/0165-2370(84)80008-X

[7] Zhou, J.B., Qiao, Y., Wang, W.X., Leng, E.W., Huang, J.C., Yu, Y., and Xu, M.H. (2016) "Formation of styrene monomer, dimer, and trimer in the primary volatiles produced from polystyrene pyrolysis in a wire mesh reactor," *Fuel*, 182:333-339, http://dx.doi.org/10.1016/j.fuel.2016.05.123

[8] Xue, Y., Zhou, S., Brown, R.C., Kelkar, A. and Bai, X.L. (2015) "Fast pyrolysis of biomass and waste plastic in a fluidized bed reactor," *Fuel*, 156:40-46, http://dx.doi.org/10.1016/j.fuel.2015.04.033

[9] Stoliarov, S.I. and Li, J. (2016) "Parameterization and validation of pyrolysis models for polymeric materials," *Fire Technology*, 52:1:79-91, http://dx.doi.org/10.1007/s10694-015-0490-1

[10] Di Blasi, C., (2008) "Modeling chemical and physical processes of wood and biomass pyrolysis," *Progress in Energy and Combustion Science*, 34:47-90, http://dx.doi.org/10.1016/j.pecs.2006.12.001

[11] Lautenberger, C., Fernandez-Pello, A.C., "Pyrolysis modeling, thermal decomposition, and transport processes in combustible solids," in: M. Faghri, B. Sunden (Eds.), *Transport Phenomena in Fires*, WIT Press, 2008, p. 209–259, http://dx.doi.org/10.2495/9781845641603/06

[12] Moghtaderi, B. (2006) "The state-of-the-art in pyrolysis modeling of lignocellulosic solid fuels," *Fire and Materials*, 30:1–34, http://dx.doi.org/10.1002/fam.891

[13] Lyon, R.E. and Janssens, M.L. "Polymer flammability," DOT/FAA/AR-05/14, 2005.

[14] Glasstone, S. and Dolan, P.J., *The Effects of Nuclear Weapons*, United States Department of Defense and the United States Department of Energy, 1977, p. 287-289.

[15] Kruse, T.M., Woo, O.S., Wong, H., Khan, S.S. and Broadbelt, L.J. (2002) "Mechanistic Modeling of Polymer Degradation: A Comprehensive Study of Polystyrene," *Macromolecules*, 35:7830-7844, http://dx.doi.org/10.1021/ma020490a

[16] Faravelli, T., Pinciroli, M., Pisano, F., Bozzano, G., Dente, M. and Ranzi, E. (2001) "Thermal Degradation of Polystyrene," *J. Anal. App. Pyrol.*, 60:103-121, http://dx.doi.org/10.1016/S0165-2370(00)00159-5

[17] Bockhorn, H., Hornung, A., Hornung, U. and Lochner, S. (2000) "Pyrolysis of Polystyrene as the Initial Step in Incineration, Fires, or Smoldering of Plastics: Investigations of the Liquid Phase," *Proceedings of the Combustion Institute*, 28:2667-2673, http://dx.doi.org/10.1016/S0082-0784(00)80686-4

[18] Kannan, P., J.J. Biernacki, D.P. Visco, Jr., "Fast Pyrolysis Kinetics of Expanded Polystyrene Foam," Wiley InterScience online publication, (2009), http://dx.doi.org/10.1002/aic.12092

[19] Kannan, P., Biernacki, J.J. and Visco Jr., D.P. (2007) "A Review of Physical and Kinetic Models of Thermal Degradation of Expanded Polystyrene Foam and Their Application to the Lost Foam Casting Process," *J. Anal. App. Pyrol.*, 78:162-171, http://dx.doi.org/10.1016/j.jaap.2006.06.005

[20] Kannan, P., J. J. Biernacki, D. P. J. Visco, and W. Lambert, (2009) "Kinetics of Thermal Decomposition of Expandable Polystyrene in Different Gaseous Environments," *J. Anal. App. Pyrol.*, 84:139-144, http://dx.doi.org/10.1016/j.jaap.2009.01.003